Journal of General Virology (2009), **90**, 854–862 **DOI** 10.1099/vir.0.005868-0

ERK MAP kinase-activated Arf6 trafficking directs coxsackievirus type B3 into an unproductive compartment during virus host-cell entry

David Marchant, Alhousseynou Sall, Xiaoning Si, Thomas Abraham, Winnie Wu, Zongshu Luo, Tamar Petersen, Richard G. Hegele and Bruce M. McManus

Correspondence
Richard G. Hegele
rhegele@mrl.ubc.ca
Bruce M. McManus
bmcmanus@mrl.ubc.ca

The James Hogg iCAPTURE Centre for Cardiovascular and Pulmonary Research, Departments of Pathology and Laboratory Medicine, The University of British Columbia, Room 166 Burrard Building, St Paul's Hospital, 1081 Burrard Street, Vancouver, BC V6Z 1Y6, Canada

Received 24 July 2008
Accepted 7 December 2008

Clathrin- and caveolae-mediated endocytosis have been implicated in the productive entry of many viruses into host cells. ADP-ribosylation factor 6 (Arf6)-dependent endocytosis is another endocytosis pathway that traffics from the cell surface and it is the only Arf that traffics at the plasma membrane. However, little is known about Arf6-dependent trafficking during virus entry. This study showed that coxsackievirus type B3 (CVB3) associated with decay-accelerating factor in non-polarized HeLa cells can be redirected into non-productive compartments by Arf6-dependent internalization, thus restricting infection. Overexpression of wild-type (WT) and constitutively active (CA) Arf6 in HeLa cells resulted in a 2.3- and 3.6-fold decrease in infection, respectively. A dominant-negative inhibitor of Arf6 recovered restriction of infection by WT-Arf6 and CA-Arf6. RNA interference of endogenous Arf6 resulted in a 3.3-fold increase in CVB3 titre in HeLa cells. It was shown that coxsackie–adenovirus receptor (CAR) ligation by virus or CAR-specific antibody could activate extracellular signal-regulated kinase (ERK) of the mitogen-activated protein kinase family and lead to Arf6-mediated viral restriction. In the absence of ERK activation, CVB3 internalization into early endosomes was inhibited and subsequent infection was reduced, but Arf6-mediated restriction was also abolished. In conclusion, receptor-mediated signalling enhances CVB3 entry whilst also activating non-productive pathways of virus entry; thus, virus infection is an equilibrium of productive and non-productive pathways of entry.

INTRODUCTION

Coxsackievirus type B3 (CVB3) infects polarized intestinal epithelium via caveolae in order to traverse the tight junction (Coyne & Bergelson, 2006) and subsequently gain access to the host circulation from the gut. Once in the circulation, CVB3 can infect a myriad of cell types, including those in the gut, liver, pancreas and heart. Non-polarized cells can be infected, and virus entry into these cells may occur via clathrin-coated pits and the early endosome network (Chung *et al.*, 2005).

Decay-accelerating factor (DAF), the CVB3 co-receptor, has been shown to traffic into high-lipid raft compartments called glycosylphosphatidylinositol (GPI)-anchored protein-enriched early endosomal compartments (Sabharanjak *et al.*, 2002), and coxsackie–adenovirus receptor (CAR) has been shown to reside with low-density lipoprotein receptor in a separate lipid-raft compartment (Ashbourne Excoffon *et al.*, 2003). This discordance of trafficking and compartmentalization is consistent with the GPI-linked nature of DAF and the fact that CAR is a transmembrane protein. Recently, ADP-ribosylation factor 6 (Arf6)-dependent endocytosis has been shown to traffic GPI-linked proteins (Karacsonyi *et al.*, 2007), such as the CVB3 co-receptor DAF. Arf6-mediated endocytosis is a lipid-raft and non-raft endocytosis pathway that cycles at the plasma membrane and is involved in the recycling of major histocompatibility complex class I to and from the cell surface. Activation of Arf6 can also lead to membrane ruffling, cell spreading, cell migration and turnover of adherens junctions (reviewed by Donaldson, 2003). We investigated Arf6, as DAF has been shown to traffic via this endocytosis pathway (Karacsonyi *et al.*, 2007; Naslavsky *et al.*, 2004) and we wanted to know what effect(s) alterations in Arf6 activity had on CVB3 entry and infectivity.

Caveolae and clathrin-coated pits are common pathways for the entry of viruses (Sieczkarski & Whittaker, 2002). However, other endocytic pathways exist and, indeed, may internalize some virus simultaneously into 'dead-end' or

non-productive virus entry pathways, as has been described previously (Marchant *et al.*, 2005). We investigated Arf6-mediated endocytosis as a candidate for the diversion of CVB3, during entry, into a non-productive pathway. Recently, Mercer & Helenius (2008) reported that Arf6 can inhibit the entry of vaccinia virus into host cells.

The ability of endocytosis to direct viruses into non-productive pathways has been described for human immunodeficiency virus (HIV) types 1 and 2 (Marchant *et al.*, 2005). This pathway was described as a pH-independent lipid-raft endocytic process, but no particular pathway was identified. Here, we used CVB3 infection of HeLa cells as a model to demonstrate that extracellular signal-regulated kinase (ERK)-mediated signalling can activate Arf6-dependent endocytosis and cause restriction of virus entry.

METHODS

Viruses and cells. CVB3 Kandolf strain (CVB3-Kan) and a molecular clone of CVB3 Woodruff (pH3; GenBank accession no. U57056) containing an enhanced green fluorescent protein (eGFP) expression cassette (eGFP–CVB3-Woodruff) described previously (Feuer *et al.*, 2002; Slifka *et al.*, 2001) were used in this study. The eGFP–CVB3-Woodruff virus was provided by Ralph Feuer and J. Lindsay Whitton (The Scripps Institute, La Jolla, CA, USA). eGFP expression from virus molecular clones allows rapid detection of virus replication, and detection of eGFP with a flow cytometer is more objective than manual counting of plaques. Results for infectivity experiments were performed on a series of virus dilutions from an m.o.i. of 0.001 to 1. Imaging experiments were conducted with both the pH3 molecular clone and Kandolf virus to confirm that these observations represented CVB3 replication in general.

HeLa and 293T cells were grown, and all treatments were performed, in Dulbecco's modified Eagle's medium with 10 % fetal bovine calf serum.

Viral vector and pseudotype production. The HIV vector pCSGW and packaging construct p8.91 have been described previously (Demaison *et al.*, 2002; Zufferey *et al.*, 1997). The vesicular stomatitis virus envelope G protein (VSV-G) construct pMDG has been described previously (Yee *et al.*, 1994). VSV-G-pseudotyped HIV-1 vectors [HIV(VSV)] were produced by three-plasmid transfection of 293T cells (Towers *et al.*, 2000).

Flow cytometry. Cells infected with 10-fold dilutions of eGFP–CVB3-Woodruff and lentivirus vector pseudotypes (m.o.i. 0.001–1) were harvested with 5 mg trypsin ml^{-1}/5 mM EDTA and fixed with 3.6 % formaldehyde at the peak of GFP expression, prior to cell lysis. This optimal time frame proved to be between 8 and 10 h post-infection (p.i.) for eGFP–CVB3-Woodruff and at 48 h for HIV(VSV) vector pseudotypes, and 2.0×10^4 cells were enumerated with a Beckman Coulter EPICS XL-MCS flow cytometer.

Antibodies and inhibitors. Rabbit anti-haemagglutinin (HA) polyclonal antibody was purchased from Sigma, anti-enterovirus VP1 monoclonal antibody (mAb) from Dako and a rabbit anti-β-catenin antibody from Cell Signaling Technology. Total ERK and phospho-ERK [phospho-p44/42 mitogen-activated protein (MAP) kinase (Thr202/Tyr204) rabbit mAb] antibodies were purchased from Cell Signaling Technology. The ERK inhibitor U0126 (10 μM working concentration) was from Cell Signaling Technology. Anti-DAF and anti-CAR mAbs used in ERK signalling neutralization studies were from Santa Cruz Biotechnology and Upstate Biotechnology, respectively. HA expression by the Arf6 constructs was detected with a rabbit polyclonal antibody and an Alexa Fluor 405-conjugated goat anti-rabbit secondary antibody (Invitrogen). Polyclonal anti-DAF (Santa Cruz) and polyclonal anti-early endosome antigen 1 (EEA1; Calbiochem) were detected with either Alexa Fluor 488 or 594 conjugated to donkey anti-goat (for DAF) or goat anti-rabbit (for EEA1) secondary antibodies.

Receptor neutralization of ERK signalling. Experiments were performed at 37 °C only. HeLa cells were treated with an anti-DAF or anti-CAR mAb at a 1 : 1000 dilution (200 ng ml^{-1}) for 30 min prior to and during CVB3 infection at an m.o.i. of 10. A higher concentration (1 : 50; 4 μg ml^{-1}) of antibody was added to cells, alone, to activate signalling via antibody–receptor binding. Cells were harvested with protein lysis buffer [10 mM HEPES (pH 7.4), 50 mM $Na_4P_2O_7$, 50 mM NaF, 50 mM NaCl, 5 mM EDTA, 5 mM EGTA, 1 mM Na_3VO_4, 0.5 % Triton X-100, 10 μg leupeptin ml^{-1} and 1 mM PMSF] on ice at 15 min p.i. and lysates were probed by Western blotting for phospho-(pThr202/pTyr204) ERK MAP kinase and total ERK.

Plasmid and RNAi transfection. Plasmids were transfected into 80 % confluent cells using Fugene (Roche) following the manufacturer's instructions. The plasmid transfection efficiency was determined as 91.3 ± 6.2 % by flow cytometry of a GFP-expressing plasmid, from three independent experiments run in parallel with the wild-type (WT) and mutant Arf6 experiments.

Dominant-negative (DN) T27N Arf6, constitutively active (CA) Q67L Arf6 and DN dynamin K44A mutants were provided by Mark Marsh (MRC Laboratory for Molecular Cell Biology and Cell Biology, London, UK). Wild-type Arf6 was constructed from the DN mutant by reversion mutation of the DN asparagine mutation at aa 27 back to a WT threonine using the GeneTailor Site-Directed Mutagenesis System (Invitrogen). The DN-Arf6 and CA-Arf6 mutants tagged with HA have been described previously (Peters *et al.*, 1995), cloned into pSRα (Dyer *et al.*, 2007).

Oligofectamine (Invitrogen) was used for transient RNAi transfection, following the manufacturer's instructions. The Arf6 small interfering (si)RNA oligonucleotides used were as follows: Arf6 oligonucleotide 1, 5′-GGGAGAUGAGGGACGCCAUAAUCCT-3′; Arf6 oligonucleotide 2, 5′-GGAGGCAGCGCACCGAGUUCCCGCG-3′; and a scramble negative oligonucleotide, 5′-CUUCCUCUCUUUCUCUCCCUUGUGA-3′.

Immunofluorescence microscopy. Immunofluorescence of coxsackievirus has been described previously (Coyne & Bergelson, 2006). Briefly, cells were fixed by addition of 3 : 1 methanol : acetone at room temperature for 2 min. Cells were blocked with 1 % BSA in PBS or blocked and permeabilized with 0.1 % Triton X-100/1 % BSA in PBS for 10 min at room temperature. Primary antibodies were added at a 1 : 100 dilution at room temperature for 2 h. Cellular markers were stained with goat anti-rabbit or donkey anti-goat secondary antibodies conjugated to Alexa Fluor 488 or 594, at a dilution of 1 : 400. The HA tag of the Arf6 constructs was detected with a rabbit polyclonal antibody against HA (Sigma) and stained with a goat anti-rabbit Alexa Fluor 405-conjugated secondary antibody (Invitrogen). For the experiments that required goat (DAF) and rabbit (CA-, DN- and WT-Arf6–HA) antibody detection, the goat anti-rabbit secondary antibody was added after the donkey anti-goat antibody, with an additional washing step, to prevent secondary antibody cross-reactivity. Virus was stained with a goat anti-mouse biotinylated secondary antibody (Vector Technologies) at a dilution of 1 : 400. Streptavidin-conjugated 655 quantum dots (Invitrogen) were added at a dilution of 1 : 1000 for 1 h at room temperature. Each step was followed by three washes in PBS. Alternatively, to improve clarity, virus was stained using Alexa Fluor 488-conjugated secondary antibodies and cellular markers were stained using Alexa Fluor 594-

and 405-conjugated secondary antibodies as described above. Samples were mounted under a coverslip in Vectashield containing DAPI (Vector laboratories).

Image acquisition, three-dimensional modelling and rendering. Immunofluorescence confocal microscopy was conducted using an AOBS Leica Confocal TCS SP2 microscope (63×, NA 1.2). Lambda scans were performed throughout the experiments to confirm the specificity of the Alexa Fluor and quantum dot signal profiles. Image stacks (90–140 × 512 × 512 pixels; three-frame mean) were collated using Impro*vision* Volocity software, with minor brightness and contrast adjustment (not greater than 15 % of original values).

Pearson's correlations were obtained using Volocity software. Channels 2 [green (VP1)] and 3 [red (EEA1)] from 90–140 × 512 × 512 image stacks were subject to correlation.

Statistical analysis. SD was used to represent data distribution. Student's *t*-test was used to determine statistical significance.

RESULTS

Arf6 uptake of CVB3 during entry is detrimental to infection

CVB3 enters HeLa cells via a dynamin-dependent pathway (Chung *et al.*, 2005). To confirm the endocytic uptake of CVB3 during entry, we monitored the entry of a dynamin-dependent VSV-G-pseudotyped retroviral vector, (VSV)HIV, in parallel with CVB3 during WT dynamin and DN dynamin K44A expression. Fig. 1 shows that dynamin K44A significantly decreased CVB3 infectivity from 5.0×10^5 to 1.8×10^5 (P=0.05) infectious units (IU) ml^{-1}. This constituted a 2.8-fold reduction in infectivity. The infectivity of the (VSV)HIV vector, as described previously (Pelkmans *et al.*, 2005; Sun *et al.*, 2005), was correspondingly decreased 3.6-fold (P=0.0004). These results suggested that our results are consistent with what has been shown previously for CVB3 regarding dynamin dependence (Chung *et al.*, 2005).

Endocytosis can result in the productive entry of viruses into host cells (Sieczkarski & Whittaker, 2002). However, lipid raft-mediated endocytosis pathways have also been implicated in virus entry restriction (Marchant *et al.*, 2005). We focused on Arf6-mediated endocytosis as it has been shown to traffic at the plasma membrane and Arf6-mediated endocytosis is thought to mediate the trafficking of lipid rafts at the cell surface (Balasubramanian *et al.*, 2007). Thus, we expressed DN-Arf6 (T27N), CA-Arf6 (Q67L) and WT-Arf6 in HeLa cells and monitored CVB3 infection (Fig. 2). The control for Arf6 activity confirmed that CA- and DN-Arf6 inhibited the internalization of β-catenin upon exposure to 5 mM EDTA (Fig. 2a) (Palacios *et al.*, 2001).

HeLa cells transfected with WT-, DN- and CA-Arf6 were infected with eGFP–CVB3-Woodruff. We found that CA-Arf6 decreased infection 3.0-fold, from 1.0×10^7 to 3.3×10^6 IU ml^{-1} (P=0.009; Fig. 2b). We recovered CVB3 infection using the reduced Arf6 trafficking activity of the GDP-bound DN-Arf6 mutant to 8.1×10^6 IU ml^{-1}, which constituted a 2.5-fold recovery of infection over the CA-Arf6 mutant.

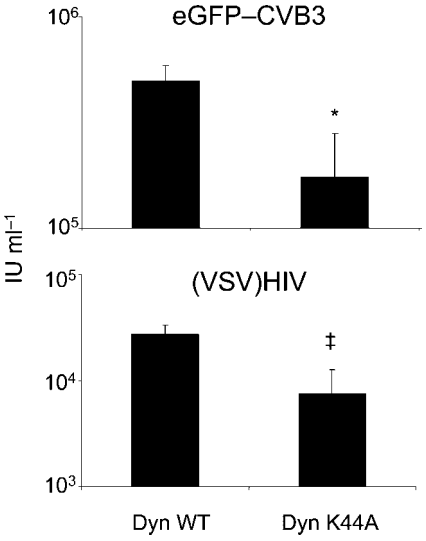

Fig. 1. Dynamin-dependent entry of CVB3 into cells. Entry of a dynamin- and pH-dependent VSV-G-protein pseudotyped retroviral vector, (VSV)HIV, was monitored in parallel with eGFP–CVB3-Woodruff during WT and K44A dynamin expression. CVB3 and (VSV)HIV were added to dynamin K44A- and WT-transfected cells and fixed at 8 and 48 h p.i., respectively, and the number of IU ml^{-1} was enumerated by flow cytometry. Note the statistically significant decrease in eGFP–CVB3-Woodruff in dynamin K44A-transfected cells (*P<0.05; ‡P<0.001). Results are representative of two independent experiments.

Overexpression of Arf6 via a WT-Arf6 mutant decreased infection to 4.4×10^6 from 1.0×10^7 IU ml^{-1} in control HeLa cells (P=0.009), which constituted a 2.3-fold reduction in infectivity compared with control infection.

We silenced endogenous Arf6 expression in HeLa cells to determine the effect of endogenous Arf6 levels on CVB3 infection (Fig. 2c, inset). Arf6 was silenced using siRNA and cells were infected 2 days later (Fig. 2c). We observed a 3.0- and 2.6-fold recovery of CVB3 infection in Arf6-silenced HeLa cells using oligonucleotides 1 and 2, respectively, compared with the scramble oligonucleotide-treated control cells.

A fraction of co-localized CVB3 and DAF is sequestered to discrete regions of HeLa cells overexpressing WT-Arf6

Arf6-mediated endocytosis is responsible for some GPI-linked protein trafficking activity (Naslavsky *et al.*, 2004). Therefore, we imaged the interaction of CVB3 with its GPI-linked co-receptor, DAF, at early time points p.i. in HeLa cells overexpressing WT-Arf6. We used a VP1 mAb, a biotin-conjugated secondary antibody and quantum dots to enhance the signal-to-noise ratio and narrow the emission wavelengths of CVB3 imaging during virus entry. At 10 min p.i., we observed CVB3 and DAF sequestered into discrete regions, distant from the nucleus (Fig. 3a, white arrows), in WT-Arf6-expressing cells. We noted that the untransfected

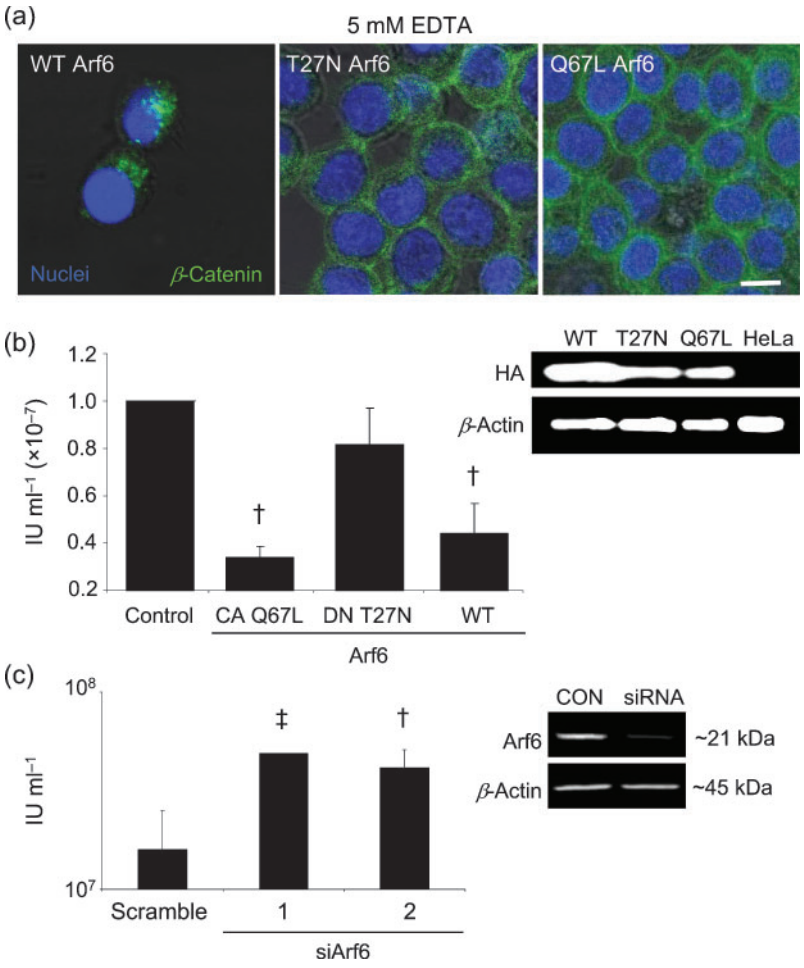

Fig. 2. Arf6 activity mediates restriction of CVB3 during host-cell entry. (a) DN-Arf6 and CA-Arf6 inhibit the internalization of β-catenin after treatment with 5 mM EDTA. HeLa cells were treated with 5 mM EDTA for 30 min prior to fixation and staining. Images were captured using a Leica SP2 confocal microscope. Bar, 10 μm. (b) DN-Arf6-expressing cells recover WT-Arf6-mediated restriction of CVB3 relative to control cells. HeLa cells were transfected with DN-, CA- or WT-Arf6, washed the following day and infected at 48 h post-transfection. Cells were fixed and the number of IU ml^{-1} was enumerated by flow cytometry 8 h later. Alternatively, cells were harvested with protein lysis buffer and subjected to an anti-HA and anti-actin Western blot (shown as a positive image from a ChemiGenius blot and gel imaging system). (c) Silencing of endogenous Arf6 expression in HeLa cells recovers eGFP–CVB3-Woodruff infection in HeLa cells. HeLa cells were silenced for Arf6 expression using siRNA oligonucleotides directed against Arf6. Cells were transfected with Arf6 RNA oligonucleotides 1 or 2 or the scramble oligonucleotide (CON), washed the following day and infected with CVB3 at 48 h post-transfection. Alternatively, cells were harvested with protein lysis buffer and subject to Western blotting to detect Arf6 and actin. †$P<0.01$; ‡$P<0.001$. Results are representative of three independent experiments.

cells demonstrated proximal virus/DAF nucleus localization (arrow head) at 10 min p.i. As WT-Arf6 expression resulted in a loss of infectivity, we considered the sequestering of CVB3 into pockets away from perinuclear regions as a mechanism of virus entry restriction.

We also imaged CVB3 entry using secondary antibodies conjugated with Alexa Fluor 488. This dye has a lower signal-to-noise ratio than quantum dots, but we noted that the clarity of the images was greater. Fig. 3(b) is a 60 min time course of CVB3 entry. At 0 min p.i., we saw a similar pattern of VP1 staining on WT-Arf6-transfected and -untransfected cells. However, at 30 and 60 min p.i., there was a brighter pattern of CVB3 VP1 staining on WT-Arf6-transfected cells (arrows). The untransfected cells showed a fainter but proximal nuclear localization of CVB3 (arrow heads).

Virus ligation of the CAR receptor, but not the DAF co-receptor, activates ERK MAP kinase

Trafficking of the Arf6-dependent endocytosis pathway can be enhanced by ERK MAP kinase activation (Robertson *et al.*, 2006) and ERK MAP kinase activity can be triggered by Arf6 (Tushir & D'Souza-Schorey, 2007). The importance of ERK signalling during CVB3 infection has been demonstrated *in vitro* (Luo *et al.*, 2002) and *in vivo* (Opavsky *et al.*, 2002), but the precise mechanism of activation has not been elucidated.

Fig. 4 shows a Western blot of phospho-(pThr202/pTyr204) ERK MAP kinase and total ERK at 15 min p.i. The results showed that virus activated ERK during entry but that ERK activation was inhibited with an anti-CAR mAb at a 1 : 1000 dilution (200 ng ml^{-1}). In contrast, the anti-DAF mAb had little effect on activation of ERK. By raising the concentrations of the DAF and CAR antibodies to 1 : 50 (4 μg ml^{-1}), we were able to activate ERK with anti-CAR antibody alone but not with anti-DAF antibody. These results show for the first time that CVB3 activates ERK via its primary CAR but not its DAF co-receptor on HeLa cells during virus entry.

Additionally, we noted in every experiment conducted that the anti-DAF mAb treatment decreased the basal ERK activity to undetectable levels (Fig. 4).

Inhibition of ERK activation during CVB3 entry reduces VP1 to EEA1 co-localization during virus entry

A previous study has shown how ERK activation can trigger uptake by clathrin-mediated endocytosis (Khundmiri *et al.*, 2004). As CVB3 has been reported to enter HeLa cells via

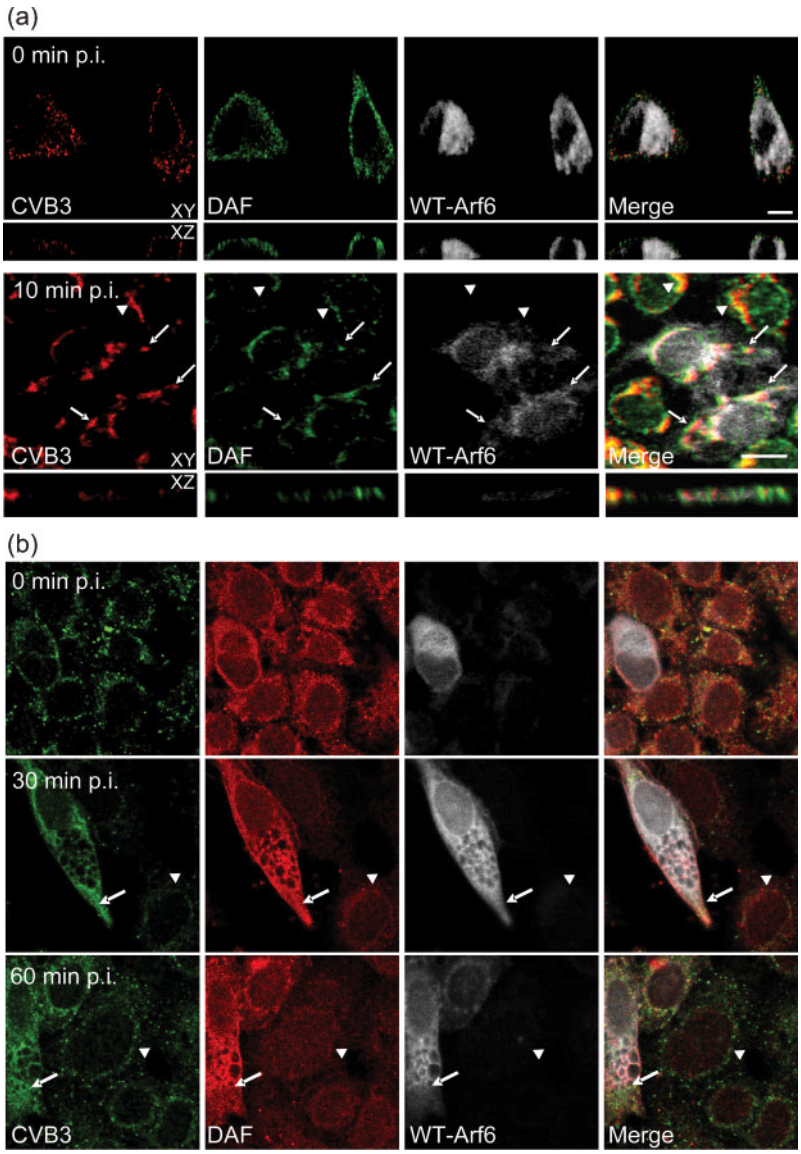

Fig. 3. Arf6 expression results in sequestering of CVB3 away from perinuclear regions during entry. HeLa cells expressing WT-Arf6 were infected with CVB3 on ice for 1 h, warmed to 37 °C and fixed, and the virus was stained with 655 nm quantum dots at 0 and 10 min p.i. (a) or with Alexa Fluor 488 at 0, 30 and 60 min p.i. (b) to confirm the imaging method in (a). Images were acquired with a Leica SP2 confocal microscope. Arrows indicate virus sequestered into tubular processes, distant from the nucleus, in WT-Arf6-transfected cells. Arrowheads demonstrate virus/DAF proximal to the nucleus of untransfected cells. Results are representative of two independent experiments for each quantum dot and Alexa Fluor 488 virus-staining method.

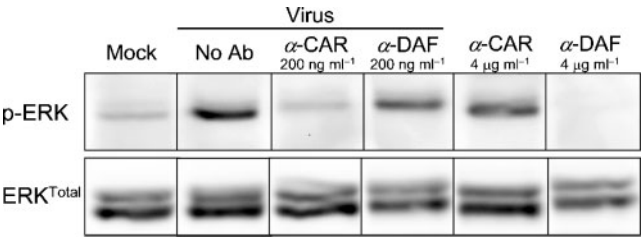

Fig. 4. ERK activation can be inhibited by blocking the virus–CAR interaction or activated by adding high concentrations of anti-CAR, but not anti-DAF, antibody. HeLa cells were treated with anti-DAF or anti-CAR mAb for 30 min prior to and during CVB3 infection. Cells were harvested with protein lysis buffer on ice at 15 min p.i. and lysates were probed for phospho-(pThr202/pTyr204) ERK MAP kinase (upper panels) and total ERK (lower panels). The image shown is the product of one Western blot and was rearranged for ease of presentation. Results are representative of three independent experiments.

clathrin-mediated endocytosis and EEA1-positive endosomes (Chung *et al.*, 2005), we analysed a time course of CVB3 infection by staining, including a DMSO vehicle control and U0126 (10 μM)-treated cells, for EEA1 and VP1, at 0, 30 and 60 min p.i. (Fig. 5). Transport of CVB3 into EEA1 during entry has been demonstrated previously (Chung *et al.*, 2005). Consistent with these findings, we noted that EEA1 coalesced in the control cells at 30 and 60 min p.i. (Fig. 5b and c). The U0126-treated infection time courses in Fig. 5(b and c) showed that there was less coalescence of EEA1 at 30 and 60 min p.i., respectively. In addition, there also appeared to be less VP1 to EEA1 co-localization at these same time points.

We used Pearson's correlation to quantify the co-localization of pixels in the CVB3 VP1 channel to pixels in the EEA1 channel during CVB3 entry. A Pearson's correlation of 1 indicates that every pixel in a given channel is correlated/co-localized with the pixels in the second

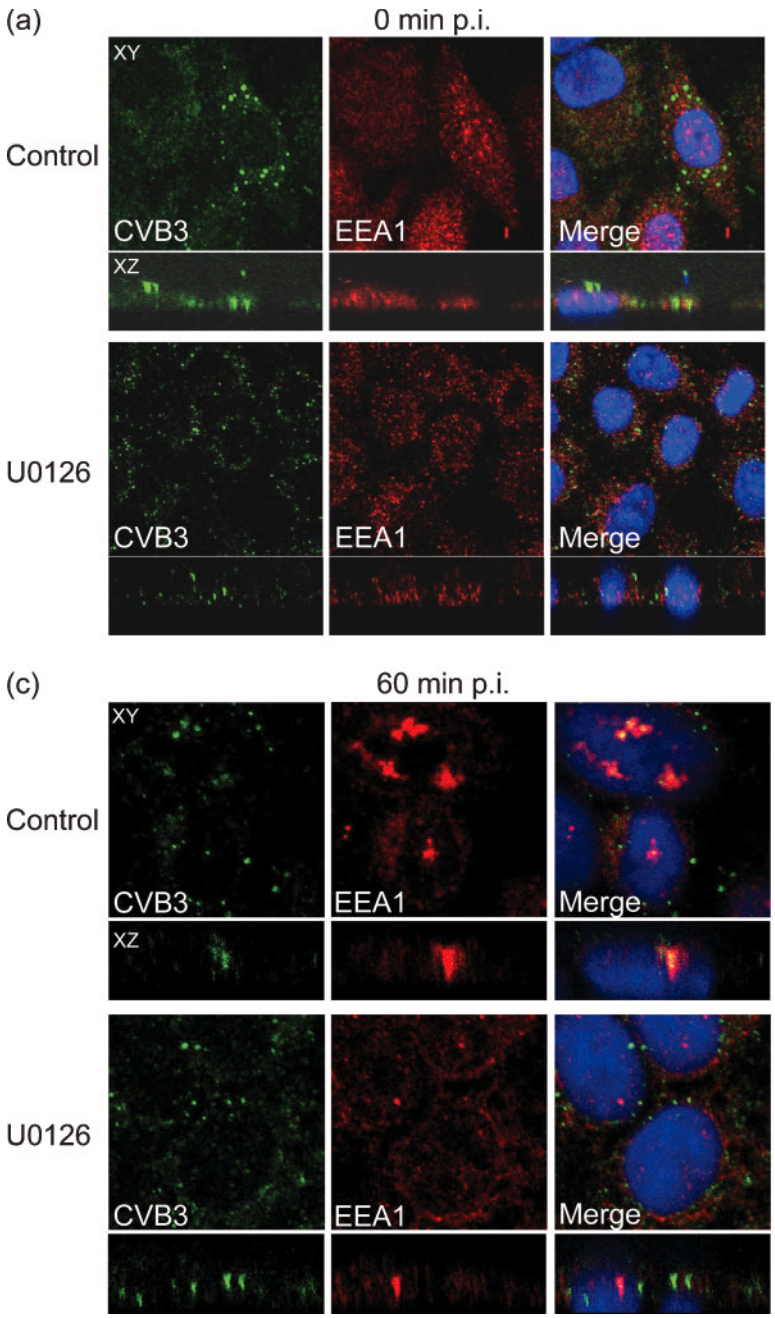

Fig. 5. Inhibition of virus-induced ERK MAP kinase activation by U0126 inhibits coalescence of, and virus entry into, EEA1 endosomes at 60 min p.i. (a–c) CVB3 was bound to cells on ice for 60 min in the presence or absence of U0126 and warmed to 37 °C for the indicated period of time. Control cells were treated with DMSO vehicle only. Cells were fixed at 0 min (a), 30 min (b) and 60 min (c) p.i. and stained for virus (Alexa Fluor 488), EEA1 (Alexa Fluor 594) and nuclei (DAPI). Cells were imaged using a Leica SP2 AOBS confocal microscope. (d) Graph of Pearson's correlation of EEA1 and VP1 co-localization (*y*-axis) at 0 and 60 min p.i. from two independent experiments. **P*=0.05.

channel. A correlation of 0 indicates no co-localization of pixels between the different channels. Fig. 5(d) shows the Pearson's correlation of the VP1 channel (Alexa Fluor 488) to the EEA1 channel (Alexa Fluor 594) at 0 and 60 min p.i. As expected, the Pearson's correlation of VP1 to EEA1 was similar between the control and U0126-treated cells at 0 min p.i. However, at 60 min p.i., the Pearson's correlation of the control cells increased to 0.39 compared with 0.22 in the U0126-treated cells (P=0.05). These results suggested that ERK inhibition by U0126 treatment inhibits the uptake of CVB3 into the early endosome.

We treated HeLa cells, expressing WT-, DN- and CA-Arf6, with U0126 for 30 min prior to infection and for the first 1 h of CVB3 infection. This experiment was designed so that ERK activation would be targeted during the entry phase of virus infection only. Cells were harvested 8–10 h later for enumeration of infection by flow cytometry. As discussed earlier, and shown in Fig. 6(a), the DN-Arf6 mutant recovered infection (2.3×10^5 IU ml^{-1}) restricted by the WT-Arf6 mutant (1.2×10^5 IU ml^{-1}; P=0.02). Fig. 6(a) also shows how infection was decreased when ERK activation was inhibited during entry of CVB3, from 4.1×10^5 to 1.5×10^5 IU ml^{-1}, a 2.7-fold loss of infectivity, when ERK was inhibited (Fig. 6b). However, the WT-Arf6- and DN-Arf6-expressing cells exhibited similar titres of 1.1×10^5 and 1.3×10^5 IU ml^{-1} upon treatment with U0126 (P=0.5; Fig. 6a). These titres were within 1.3- and 1.2-fold of the control HeLa cells, respectively. This suggests that CVB3 is not further restricted by Arf6 in the absence of ERK activation. However, CA-Arf6 should remain active even in the absence of ERK stimulation and should therefore restrict CVB3 further with U0126 treatment. Indeed, U0126-treated CA-Arf6-expressing cells were infected to a titre of 5.3×10^4 IU ml^{-1} whereas the U0126-treated control cells were infected to a titre of 1.5×10^5 IU ml^{-1} (P=0.02; Fig. 6a). This constituted a further 2.8-fold reduction in infectivity in the U0126-treated CA-Arf6-expressing cells compared with the U0126-treated control cells (Fig. 6b).

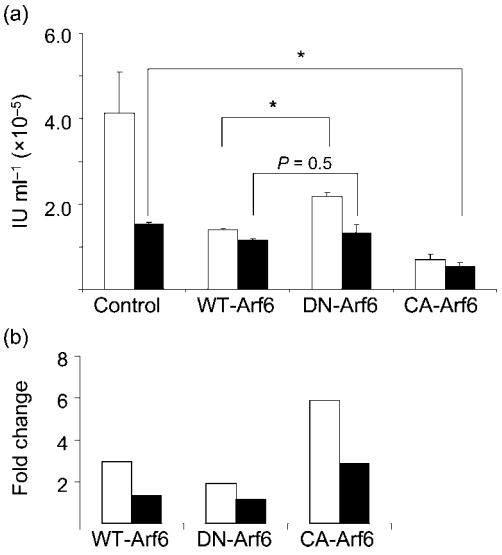

Fig. 6. Inhibition of ERK activation with U0126 eliminates Arf6-mediated restriction of CVB3. (a) HeLa cells were transfected with WT-, DN- or CA-Arf6 and infected with CVB3 2 days later. U0126 ERK inhibitor (filled bars) or DMSO vehicle (empty bars) was added for the first hour of infection to target the virus-entry window. Infection was enumerated by flow cytometry at 8 h p.i. (b) Fold changes in infection relative to the corresponding U0126-treated or untreated transfection control in (a). Infection (IU ml^{-1}) in the control transfection cells was divided by infection in Arf6-transfected cells (empty bars) or U0126-treated cells (filled bars). *P<0.05. Results are representative of four independent experiments.

DISCUSSION

CVB3 can be sequestered by Arf6 trafficking activity into a compartment that does not support replication. By imaging early virus entry events, it appears that virus is caught within Arf6-dependent compartments that sequester virus and prevent trafficking to perinuclear regions that better support virus replication. However, virus also triggered, via CAR ligation, ERK MAP kinase signalling activity, which enhanced the productive internalization of CVB3 into the cell. Paradoxically, this same ERK signalling activity is responsible for Arf6-mediated restriction of virus infection.

Our results support the notion that CVB3 enters EEA1-positive endosomes during entry (Chung *et al.*, 2005), and that this activity is dependent on the activation of ERK MAP kinase. However, this is not the first time that endosomal trafficking activity has been attributed to MAP kinase of ERK (MEK)/ERK activation. Phosphorylation and subsequent endocytosis of the Na^+,K^+-ATPase α_1-subunit into clathrin-coated vesicles is mediated by ERK (Khundmiri *et al.*, 2004), and the negative feedback of this process may even be mediated by localization of MEK2 to endosomes (Galperin & Sorkin, 2008).

We noted that cells expressing a WT-Arf6 construct demonstrated the greatest degree of lamellipodia-like protrusions as early as 10 min p.i., which were not evident with U0126 treatment. Results from our laboratory have shown that 10–20 min after CVB3 infection is the time when the majority of entry-phase ERK activation takes place (Luo *et al.*, 2002; Si *et al.*, 2005) and when ERK has been shown to enhance Arf6 activity (Robertson *et al.*, 2006), resulting in cortical actin rearrangement and cell spreading (Klemke *et al.*, 1997; Song *et al.*, 1998). Imaging experiments showed VP1 protein sequestered away from perinuclear localized VP1 at 10 min p.i. in WT-Arf6-expressing cells, which we did not see in untransfected cells, so we postulated that this virus-sequestering activity by Arf6 results in CVB3 entry restriction.

The CVB3 restriction activity of the Arf6 mutants was discordant with the inhibition of β-catenin internalization during EDTA treatment. Our results showed that the DN-Arf6 mutant recovered infection restricted by the CA- and WT-Arf6 mutants; however, the DN and CA mutants both

perturbed the internalization of β-catenin. These data indicate different activities of Arf6-mediated internalization. The CA-Arf6 mutant has been reported to produce an accumulation of Arf6-positive vesicles, not normally seen in cells expressing WT-Arf6, 'blocking recycling and vesicle convergence' (Donaldson, 2003). 'Any mutant that blocks the cycle may block Arf6 function' (Donaldson, 2003) and our results of both CA and DN mutants blocking β-catenin internalization are certainly supported by these observations. Thus, merely perturbing the action of Arf6 with the DN and CA mutants is sufficient to inhibit internalization of β-catenin, probably because the pathway into which β-catenin is normally routed is interrupted by both mutants. Therefore, we propose that the activity level of Arf6, rather than any particular compartment, can draw virus away from a clathrin-mediated endocytosis pathway and productive regions of virus replication, resulting in restriction.

The CAR-dependent activation of ERK MAP kinase appears to activate two conflicting pathways: there was elimination of virus restriction by Arf6 when we treated target cells with the ERK inhibitor U0126, but productive clathrin-mediated pathways were inhibited. Arf6 and ERK activation states may well be co-dependent as Arf6 activity can result in ERK activation (Tushir & D'Souza-Schorey, 2007), but the results obtained here support the observation that Arf6 activity is dependent on ERK activation (Robertson *et al.*, 2006).

Virus restriction by internalization into a detrimental endocytosis pathway has been described for HIV-1 and -2 (Marchant *et al.*, 2005; Marsh & Helenius, 2006) and for vaccinia virus via Arf6 (Mercer & Helenius, 2008), which are very different viruses in morphology and life cycle compared with CVB3. Interestingly, vaccinia virus (de Magalhaes *et al.*, 2001) and HIV (via CD4 ligation) (Popik *et al.*, 1998) also activate ERK MAP kinase during virus entry, which may also activate Arf6-mediated restriction during internalization. The congruity of these studies suggests that equilibrium between productive and non-productive pathways may be a common trait of virus entry. Finally, non-productive endocytosis pathways of entry may be determinants of virus tropism through restriction of virus infection.

ACKNOWLEDGEMENTS

This work was supported by grants from the Heart and Stroke Foundation of British Columbia and Yukon (B. M. M.) and the Canadian Institutes of Health Research (CIHR) (B. M. M. and R. G. H.). X. S. is supported by a CIHR IMPACT Post-Doctoral Fellowship and CIHR Michael Smith Post-Doctoral Fellowship. D. M. is supported by CIHR, IMPACT and a British Columbia Lung Association Post-Doctoral Fellowship.

REFERENCES

Ashbourne Excoffon, K. J. D., Moninger, T. & Zabner, J. (2003). The coxsackie B virus and adenovirus receptor resides in a distinct membrane microdomain. *J Virol* **77**, 2559–2567.

Balasubramanian, N., Scott, D. W., Castle, J. D., Casanova, J. E. & Schwartz, M. A. (2007). Arf6 and microtubules in adhesion-dependent trafficking of lipid rafts. *Nat Cell Biol* **9**, 1381–1391.

Chung, S. K., Kim, J. Y., Kim, I. B., Park, S. I., Paek, K. H. & Nam, J. H. (2005). Internalization and trafficking mechanisms of coxsackievirus B3 in HeLa cells. *Virology* **333**, 31–40.

Coyne, C. B. & Bergelson, J. M. (2006). Virus-induced Abl and Fyn kinase signals permit coxsackievirus entry through epithelial tight junctions. *Cell* **124**, 119–131.

de Magalhaes, J. C., Andrade, A. A., Silva, P. N., Sousa, L. P., Ropert, C., Ferreira, P. C., Kroon, E. G., Gazzinelli, R. T. & Bonjardim, C. A. (2001). A mitogenic signal triggered at an early stage of vaccinia virus infection: implication of MEK/ERK and protein kinase A in virus multiplication. *J Biol Chem* **276**, 38353–38360.

Demaison, C., Parsley, K., Brouns, G., Scherr, M., Battmer, K., Kinnon, C., Grez, M. & Thrasher, A. J. (2002). High-level transduction and gene expression in hematopoietic repopulating cells using a human immunodeficiency virus type 1-based lentiviral vector containing an internal spleen focus forming virus promoter. *Hum Gene Ther* **13**, 803–813.

Donaldson, J. G. (2003). Multiple roles for Arf6: sorting, structuring, and signaling at the plasma membrane. *J Biol Chem* **278**, 41573–41576.

Dyer, N., Rebollo, E., Domínguez, P., Elkhatib, N., Chavrier, P., Daviet, L., González, C. & González-Gaitán, M. (2007). Spermatocyte cytokinesis requires rapid membrane addition mediated by ARF6 on central spindle recycling endosomes. *Development* **134**, 4437–4447.

Feuer, R., Mena, I., Pagarigan, R., Slifka, M. K. & Whitton, J. L. (2002). Cell cycle status affects coxsackievirus replication, persistence, and reactivation in vitro. *J Virol* **76**, 4430–4440.

Galperin, E. & Sorkin, A. (2008). Endosomal targeting of MEK2 requires RAF, MEK kinase activity and clathrin-dependent endocytosis. *Traffic* **9**, 1776–1790.

Karacsonyi, C., Miguel, A. S. & Puertollano, R. (2007). Mucolipin-2 localizes to the Arf6-associated pathway and regulates recycling of GPI-APs. *Traffic* **8**, 1404–1414.

Khundmiri, S. J., Bertorello, A. M., Delamere, N. A. & Lederer, E. D. (2004). Clathrin-mediated endocytosis of Na^+,K^+-ATPase in response to parathyroid hormone requires ERK-dependent phosphorylation of Ser-11 within the α1-subunit. *J Biol Chem* **279**, 17418–17427.

Klemke, R. L., Cai, S., Giannini, A. L., Gallagher, P. J., de Lanerolle, P. & Cheresh, D. A. (1997). Regulation of cell motility by mitogen-activated protein kinase. *J Cell Biol* **137**, 481–492.

Luo, H., Yanagawa, B., Zhang, J., Luo, Z., Zhang, M., Esfandiarei, M., Carthy, C., Wilson, J. E., Yang, D. & McManus, B. M. (2002). Coxsackievirus B3 replication is reduced by inhibition of the extracellular signal-regulated kinase (ERK) signaling pathway. *J Virol* **76**, 3365–3373.

Marchant, D., Neil, S. J., Aubin, K., Schmitz, C. & McKnight, A. (2005). An envelope-determined, pH-independent endocytic route of viral entry determines the susceptibility of human immunodeficiency virus type 1 (HIV-1) and HIV-2 to Lv2 restriction. *J Virol* **79**, 9410–9418.

Marsh, M. & Helenius, A. (2006). Virus entry: open sesame. *Cell* **124**, 729–740.

Mercer, J. & Helenius, A. (2008). Vaccinia virus uses macropinocytosis and apoptotic mimicry to enter host cells. *Science* **320**, 531–535.

Naslavsky, N., Weigert, R. & Donaldson, J. G. (2004). Characterization of a nonclathrin endocytic pathway: membrane cargo and lipid requirements. *Mol Biol Cell* **15**, 3542–3552.

Opavsky, M. A., Martino, T., Rabinovitch, M., Penninger, J., Richardson, C., Petric, M., Trinidad, C., Butcher, L., Chan, J. & Liu, P. P. (2002). Enhanced ERK-1/2 activation in mice susceptible to coxsackievirus-induced myocarditis. *J Clin Invest* **109**, 1561–1569.

Palacios, F., Price, L., Schweitzer, J., Collard, J. G. & D'Souza-Schorey, C. (2001). An essential role for ARF6-regulated membrane traffic in adherens junction turnover and epithelial cell migration. *EMBO J* **20**, 4973–4986.

Pelkmans, L., Fava, E., Grabner, H., Hannus, M., Habermann, B., Krausz, E. & Zerial, M. (2005). Genome-wide analysis of human kinases in clathrin- and caveolae/raft-mediated endocytosis. *Nature* **436**, 78–86.

Peters, P. J., Hsu, V. W., Ooi, C. E., Finazzi, D., Teal, S. B., Oorschot, V., Donaldson, J. G. & Klausner, R. D. (1995). Overexpression of wild-type and mutant ARF1 and ARF6: distinct perturbations of nonoverlapping membrane compartments. *J Cell Biol* **128**, 1003–1017.

Popik, W., Hesselgesser, J. E. & Pitha, P. M. (1998). Binding of human immunodeficiency virus type 1 to CD4 and CXCR4 receptors differentially regulates expression of inflammatory genes and activates the MEK/ERK signaling pathway. *J Virol* **72**, 6406–6413.

Robertson, S. E., Setty, S. R., Sitaram, A., Marks, M. S., Lewis, R. E. & Chou, M. M. (2006). Extracellular signal-regulated kinase regulates clathrin-independent endosomal trafficking. *Mol Biol Cell* **17**, 645–657.

Sabharanjak, S., Sharma, P., Parton, R. G. & Mayor, S. (2002). GPI-anchored proteins are delivered to recycling endosomes via a distinct cdc42-regulated, clathrin-independent pinocytic pathway. *Dev Cell* **2**, 411–423.

Si, X., Luo, H., Morgan, A., Zhang, J., Wong, J., Yuan, J., Esfandiarei, M., Gao, G., Cheung, C. & McManus, B. M. (2005). Stress-activated protein kinases are involved in coxsackievirus B3 viral progeny release. *J Virol* **79**, 13875–13881.

Sieczkarski, S. B. & Whittaker, G. R. (2002). Dissecting virus entry via endocytosis. *J Gen Virol* **83**, 1535–1545.

Slifka, M. K., Pagarigan, R., Mena, I., Feuer, R. & Whitton, J. L. (2001). Using recombinant coxsackievirus B3 to evaluate the induction and protective efficacy of $CD8^+$ T cells during picornavirus infection. *J Virol* **75**, 2377–2387.

Song, J., Khachikian, Z., Radhakrishna, H. & Donaldson, J. G. (1998). Localization of endogenous ARF6 to sites of cortical actin rearrangement and involvement of ARF6 in cell spreading. *J Cell Sci* **111**, 2257–2267.

Sun, X., Yau, V. K., Briggs, B. J. & Whittaker, G. R. (2005). Role of clathrin-mediated endocytosis during vesicular stomatitis virus entry into host cells. *Virology* **338**, 53–60.

Towers, G., Bock, M., Martin, S., Takeuchi, Y., Stoye, J. P. & Danos, O. (2000). A conserved mechanism of retrovirus restriction in mammals. *Proc Natl Acad Sci U S A* **97**, 12295–12299.

Tushir, J. S. & D'Souza-Schorey, C. (2007). ARF6-dependent activation of ERK and Rac1 modulates epithelial tubule development. *EMBO J* **26**, 1806–1819.

Yee, J. K., Miyanohara, A., LaPorte, P., Bouic, K., Burns, J. C. & Friedmann, T. (1994). A general method for the generation of high-titer, pantropic retroviral vectors: highly efficient infection of primary hepatocytes. *Proc Natl Acad Sci U S A* **91**, 9564–9568.

Zufferey, R., Nagy, D., Mandel, R. J., Naldini, L. & Trono, D. (1997). Multiply attenuated lentiviral vector achieves efficient gene delivery in vivo. *Nat Biotechnol* **15**, 871–875.